Experimental Assessment of Ductile and Shear Fracture Criteria in Stainless Steel 304 According to Hooputra Model

ARTICLE INFO

Authors
Albonasser M.[1],
Badnava H.[1]*,
Nourbakhsh S.H.[2],

ABSTRACT

The accurate prediction of crack initiation and growth in manufacturing processes is crucial for minimizing production costs and enhancing the reliability of components. This study focuses on integrated experimental investigation and fracture modeling approach for ductile metals, particularly addressing the mechanisms of ductile fracture and shear localization. The importance of establishing robust damage criteria for accurate reliable numerical simulations cannot be denied. Current literature reveals a significant lack of data on shear and ductile fracture criteria for materials like stainless steel alloy 304. To address this gap, a series of experimental tests was conducted to extract the necessary coefficients for these criteria. Various sample geometries were analyzed to investigate the effects of different triaxiality stress states and loading rates on fracture initiation. The triaxiality stress states were chosen within a range of 0.2 to 2 and strain rates were applied at values of 0.02 s^{-1}, 4.5 s^{-1}, and 30 s^{-1}. A set of coefficients for modeling ductile and shear fracture was derived, taking into account the effects of loading rate and orientation. This research not only provides critical coefficients for fracture modeling but also supports the optimization of manufacturing processes in the automotive industry and other sectors, ultimately contributing to improved material performance and component reliability.

Keywords Ductile Fracture, Shear Fracture, Hooputra Model, Stress Triaxiality, Loading Rate

[1] Department of Mechanical Engineering, Behbahan Khatam Alanbia University of Technology, Behbahan, Iran
[2] Department of Mechanical Engineering, Shahrekord University, Shahrekord, Iran

Correspondence
Address: Department of Mechanical Engineering, Behbahan Khatam Alanbia University of Technology, Behbahan, Iran.
badnava@bkatu.ac.ir

CITATION LINKS

1- A continuous damage mechanics model for .... 2- Continuum theory of ductile rupture by void nucleation and .... 3- Presentation of a new 2D fast and straightforward version for .... 4- Experimental determination and numerical implementation of .... 5- A thermodynamically consistent continuum damage model for .... 6- Nonlocal damage theory. 7- Non-local damage mechanics with .... 8- Nonlocal integral formulations of .... 9- Damage, material instabilities, and failure. 10- An anisotropic gradient damage model based on .... 11- Gradient-enhanced damage modelling of .... 12- A critical comparison of nonlocal and .... 13- A non-local implicit gradient-enhanced model for .... 14- A phase-field model for cohesive fracture. 15- An h-adaptive thermo-mechanical phase field model for .... 16- A phase field model for rate-dependent ductile fracture. 17- Finite element implementation of .... 18- Phase-field modeling of coupled anisotropic plasticity–ductile fracture in .... 19- Ductile fracture modelling based on .... 20- Implementation of the phase-field method for brittle fracture and .... 21- A damage model incorporating dynamic plastic yield surface. 22- Numerical simulation of cutting and fine cutting processes by .... 23- The Influence of Pre-Mechanical Friction Stir Processing on .... 24- A smeared-crack-based field-enriched finite element method for .... 25- A new computational method for predicting ductile failure of 304L stainless steel. 26- Ductile fracture of AISI 304L stainless steel sheet in stretching. 27- Parameter identification of a mechanical ductile damage using .... 28- Comparative study of smeared crack and extended finite element method for predicting the crack propagation in concrete gravity dams. 29- An embedded strong discontinuity model for cracking of plain concrete. 30- Numerical aspects of cohesive-zone models. 31- Cohesive-zone models, higher-order continuum theories and reliability methods for computational failure analysis. 32- Extended Finite Element Formulation. 33- A comprehensive failure model for crashworthiness simulation of aluminium extrusions. 34- Fracture criteria for automobile crashworthiness simulation of wrought aluminium alloy components. 35- Fracture characteristics of three metals subjected to various strains, strain rates, temperatures and pressures. 36- The role of microstructure in shear failure.

1- Introduction

Predicting the initiation and growth of cracks in the manufacturing processes of components is critical to reduce production costs and enhancing the reliability of produced parts. Numerical fracture modeling can reduce production costs and optimize the manufacturing process. Therefore, it is necessary to consider the criteria for crack initiation and growth in numerical simulations[1]. In ductile metals, the main mechanisms leading to fracture include the nucleation, growth, and coalescence of micro-voids, known as ductile fracture[2], or shear localization, known as shear fracture. There are various approaches to modeling damage and fracture in ductile materials. All these approaches start by deriving a set of relationships to describe damage or fracture based on observed effects in the material. Generally, fracture modeling is divided into continuous and discontinuous categories. In the first approach, the physical nature of the crack is not modeled as a discontinuity; instead, a variable is used to describe the reduction in material strength due to damage based on the continuum mechanics approach. In this category, Lemaitre's damage models and Gurson's models can be mentioned[3]. In this method, a damage variable is considered that can control the degree of material strength reduction. This variable is stored as a state variable in the modeling process. In other words, the degrees of freedom in the numerical solution remain displacement (in the quasi-static case) or velocity (in the dynamic case) for temperature-independent conditions. Sadeghi Nezhad et al.[4] presented a specialized two-dimensional form of the Lemaitre model for plane stress conditions. The application of this model in the numerical simulation of the initiation and growth of ductile damage in metal sheets has been examined. Salimpour[5] studied the mechanical behavior and ductile damage of Al2024 aluminum alloy experimentally and through numerical simulation to consider the effect of stress state on damage conditions. The objective of his research was to establish a relationship between failure strain and damage state in the material. Under such circumstances, the numerical solution becomes dependent on the mesh density, and as the number of elements increases, meaning the use of smaller meshing, non-physical localization occurs[6]. Non-local methods are used to overcome this form of localization[7]. The application of this method for concrete damage is discussed in reference[8], and for plastic behavior with damage to address mesh dependency issues in reference[9]. In this context, one can refer to the research by Badnava et al.[10] in anisotropic damage modeling using the microplane method, which utilized implicit gradients to prevent localization. Other applications of non-local methods can be found in references. Peerlings and de Borst demonstrated the use of the gradient method to introduce non-local components in relations[11]. A comparison between the gradient method and the integration method in non-local modeling is provided in reference[12]. Badnava et al.[13] used this approach for modeling the unstable behavior of shape memory alloys.

The phase field method also falls into the category of methods where the crack is not modeled discretely, but rather its regularized form is considered[14]. In this method, an additional variable alongside the other degrees of freedom of the element is considered, representing the crack state in each body. Badnava et al. used this method to simulate crack initiation, crack propagation and crack coalescence by considering temperature effects[15]. On that work, an h-adaptive approached has been introduced to have a fine mesh around the crack area. They also presented the extension of this model for simulating the fracture of ductile materials[16]. Marandi et al. extended this model to include the effects of rate and temperature[17] and also in modeling fracture while considering anisotropy effects in plastic behavior[18]. Additionally, the application of this method in pressure-dependent material behavior[19] and in porous materials[20] well demonstrates the capability of this method in simulating cracks in various conditions. Ganjiani[21] presented a model for simulating the damage of ductile metals, considering the effects of loading rates using the continuum damage method. The application of this class of methods in cutting, considering large deformation effects, has been presented by Aboutalebi[22]. Finally, the effects of friction stir welding on the stress state in aluminum alloys were studied by Tavoli[23], and in Salimpour's research[4], a ductile damage model was implemented. In that research, the model coefficients were experimentally derived for aluminum alloy A12024. Finally, the smeared crack method is also included in the continues modelling category[24]. A parameter identification of a mechanical ductile damage using Artificial Neural Networks in sheet metal forming has been suggested by Abbassi et al[25] for the Gurson–Tvergaard–Needleman damage model. Ben Othmen et al.[26] has been investigated ductile fracture of AISI 304L stainless steel sheet in stretching. The have performed a numerical investigation of fracture initiation of austenitic stainless steel, AISI 304L, during a forming process. Their results demonstrated that the Rice-Tracey or Brozzo fracture criteria are reliable predictors of the onset of fracture of AISI 304L in the Erichsen test. Kim et al.[27] suggested a computational method for predicting ductile failure of 304L stainless steel using a modified Mohr–Coulomb fracture criterion that include stress triaxiality and lode angle influences. Haghani et al.[28] conducted a comprehensive review of the Smeared Crack method and the Extended Finite Element Method in simulating and modeling crack growth in concrete gravity dams.

As mentioned, in the first approach, the discontinuous nature of the crack is not considered. However, in the second approach, the crack is directly modeled as a discontinuity. This category includes modeling methods such as embedded strong discontinuity[29], cohesive zone[30], and extended finite element[31]. The numerical implementation of the cohesive zone method was investigated by de Borst[32]. In both mentioned approaches, it is necessary to consider criteria for the initiation and subsequent growth of cracks. Hooputra et al.[33], based on empirical observations, have provided criteria for predicting the initiation of shear fracture and ductile fracture. They have conducted comprehensive experimental and numerical investigations on aluminum

alloys for use in the automotive industry[34]. The extraction of coefficients for their proposed model requires a series of tests at different loading rates and stress states. Currently, there is insufficient data on these criteria for other metals. In this research, a set of experimental tests on stainless steel alloy 304 is conducted to extract the coefficients for the shear fracture and the ductile fracture criteria. Samples with different geometries are considered to investigate the effects of various triaxial stress states on the initiation of fracture. In each case, the effect of the loading rate is also examined. Finally, the coefficients for the desired criteria are extracted based on the experimental results.

2- Criteria for Fracture Initiation in Metals

In this section, the criteria for fracture initiation in metals due to ductile fracture and shear fracture are described. The presented criteria are phenomenological and are expressed based on macroscopic stress and strain responses. These criteria consider the effects of anisotropy and loading rate[33]. Temperature effects were not considered in this research.

2-1- Ductile Fracture Criterion

The mechanism for ductile fracture in metals involves the nucleation of voids, their growth, and subsequent coalescence. In most of the available models, the damage variable is considered for reducing the strength. If it equals zero, it means the material is undamaged, and if it equals one, the material has completely lost its strength. The purpose of the model is to determine the onset of damage growth from the undamaged state. The Gurson model is one of the criteria in which the volume fraction of voids in the material is expressed as a fractional component in the yield criterion[2]. Another common criterion for predicting the initiation of ductile fracture is the Johnson-Cook criterion[35]. The Johnson-Cook model is commonly suitable for very high loading rates and for considering temperature effects. The Hooputra model[33] is more suitable for parts made from sheets and profiles. In this research, the aim is to determine the coefficients of the Hooputra model. This is referred to as the damage initiation criterion. A criterion is also defined for the expansion of damage from zero to one. The ductile fracture process is a function of triaxial stress and loading rate. Phenomenological models based on critical equivalent plastic strain have been proposed. These models assume that the equivalent plastic strain at the initiation of ductile fracture is a function of triaxial stress and loading rate.

$$\bar{\varepsilon}_{eq}^{pl} = \bar{\varepsilon}_{eq}^{pl}(\eta, \dot{\bar{\varepsilon}}^{pl}) \tag{1}$$

In which $\eta = -p/q$, η represents the triaxiality of stress, p is the pressure, and q is the effective stress. Also, $\dot{\bar{\varepsilon}}^{pl}$ is the equivalent plastic strain rate. For a general strain path, the following integral criterion is used to evaluate the onset of ductile fracture:

$$w_D = \int \frac{d\bar{\varepsilon}_{eq}^{pl}}{\bar{\varepsilon}_{eq}^{pl}(\eta, \dot{\bar{\varepsilon}}^{pl})} = 1 \tag{2}$$

where w_D is the controlling variable for the initiation of ductile fracture, and its rate of change is always positive or zero to account for the irreversibility of damage. In the Hooputra model the equivalent plastic strain at the onset of fracture is defined as follows[33]:

$$\bar{\varepsilon}_{eq}^{pl} = \frac{\varepsilon_T^+ \sinh\left[c(\eta^- - \eta)\right] + \varepsilon_T^- \sinh\left[c(\eta - \eta^+)\right]}{\sinh\left[c(\eta^- - \eta^+)\right]} \tag{3}$$

where η^+ and η^- represent the triaxiality of stress in biaxial tension and compression, respectively. ε_T^+ and ε_T^- are the equivalent plastic strains at the fracture point for biaxial tension and compression, respectively, and both are independent of orientation. The effect of orientation in the above criterion is considered using the variable c. In this research, the effect of orientation relative to the rolling direction is evaluated. The relationship of the variable c based on the angle v between the rolling direction and the principal strain rate direction is expressed as follows:

$$c = k_0 + k_1 cos(2v) + k_2 cos(4v) \tag{4}$$

The coefficients k_0, k_1, and k_2 are obtained based on experimental results for directions of 0 degrees, 45 degrees, and 90 degrees, as follows[33]:

$$k_0 = (c_0 + 2c_{45} + c_{90})/4 \tag{5}$$
$$k_1 = (c_0 - c_{90})/2 \tag{6}$$
$$k_2 = (c_0 - 2c_{45} + c_{90})/4 \tag{7}$$

Using the relations (3) and (4), the fracture initiation limit diagram, i.e., the equivalent plastic strain diagram at the onset of ductile fracture as a function of stress triaxiality, can be obtained. For this purpose, the coefficients of the above relations are determined using the experiments described later.

2-2- Shear Fracture

Shear fracture occurs when a local shear deformation forms a deformation zone known as a shear band. Similar to the ductile criterion, this criterion also considers the dependency on loading rate and stress triaxiality:

$$\bar{\varepsilon}_{eq}^{pl} = \bar{\varepsilon}_{eq}^{pl}(\theta, \dot{\bar{\varepsilon}}^{pl}) \tag{8}$$

$$\theta = \frac{q + k_s p}{\tau_{max}} \tag{9}$$

Where τ_{max} is the maximum shear stress, and k_s is a material constant. According to the integral criterion, shear fracture initiation is evaluated as follows:

$$w_s = \int \frac{d\bar{\varepsilon}_{eq}^{pl}}{\bar{\varepsilon}_{eq}^{pl}(\theta, \dot{\bar{\varepsilon}}^{pl})} = 1 \tag{10}$$

Similar to the ductile fracture criterion, w_s controls the loading history and remains non-decreasing. Based on the shear criterion, the equivalent plastic strain at the point of fracture initiation is defined as follows[33]:

$$\bar{\varepsilon}_{eq}^{pl} = \frac{\varepsilon_s^+ \sinh\left[f(\theta - \theta^-)\right] + \varepsilon_s^- \sinh\left[f(\theta^+ - \theta)\right]}{\sinh\left[f(\theta^+ - \theta^-)\right]} \tag{11}$$

where θ^+ and θ^- are the values of θ in biaxial tension and compression, respectively. In this criterion, the variable f is not a function of orientation, as experimental observations indicate that shear behavior shows negligible dependency on orientation. In other words, in shear fracture, there is no need to derive orientation-dependent relations. This is further explained in the process of extracting shear fracture coefficients.

Table 1) Chemical Compositions of Stainless-steel 304.

Element	Carbon (C)	Chromium (Cr)	Manganese (Mn)	Silicon (Si)	Phosphorous (P)	Sulphur (S)	Nickel (Ni)	Nitrogen (N)	Iron (Fe)
Percent %	0.07	17.50 - 19.50	2.00	1.00	0.045	0.015	8.00 - 10.50	0.10	Balance

3- Experimental investigations

In this section, the necessary experiments for extracting material behavior parameters, ductile fracture constants, and shear fracture constants are described, followed by the presentation of the results of these experiments. The experiments were conducted on the stainless-steel alloy 304, the chemical composition of which are presented in Table 1. The aim of this research is to investigate the effects of loading rate and triaxial stress state on the ductile and shear fracture of alloy stainless steel 304. To investigate material behavior and to extract the material parameters related to the considered damage criteria, it is necessary to create different stress triaxiality states and determine the equivalent plastic strain at the fracture point for each triaxial stress value. To this end, standard tension tests, biaxial tension tests, tension tests with grooves perpendicular to the loading direction, tension tests with 45-degree grooves, and tension tests with specimens having symmetrical semi-circular notches have been conducted with a universal test machine. The dimensions of the samples, based on ASTM E8M standard, are shown in Figure 1. All specimens were extracted from the same sheet with 2 mm in thickness using a computer-controlled wire cutting device. The images of the samples produced with the wire cutting device are provided in Figure 1. It is clear that in many sheet materials produced by rolling, the behavior varies in different directions due to the effects of the rolling production process and the alteration of the material structure during this process. In this research, this effect was considered by producing test samples in different directions from the sheet and in modeling as well. Therefore, for each of the experiments, samples were prepared in the rolling direction, denoted as zero degrees, perpendicular to the rolling direction, denoted as 90 degrees, and at a 45-degree angle relative to the rolling direction.

The effect of loading direction and anisotropy in material behavior is examined using the prepared samples. In addition, the effect of loading rate on the behavior of each sample is investigated. Therefore, the experiments for each direction and for each shape of the samples are conducted at three strain rates, namely quasi-static, intermediate, and high rates, equal to 0.02 s^{-1}, 4.5 s^{-1}, and 30 s^{-1}, respectively. In the rest of this research, under the title of loading rate, it is summarized as low (rate 1), medium (rate 2), and high rates (rate 3). The tension test is performed according to the standard specimen as shown in Figure 1. The results of the uniaxial tension test for the specimen without a notch, at different loading rates, are shown in Figure 2.

In Figure 2, the results of stress-strain curves indicate that the increase in stress level from low strain rate to medium strain rate is not significant. However, the reduction in strain at the fracture point, or in other words, the percentage elongation in the sample, is quite noticeable. Additionally, both the strain variation at the fracture point and the stress level at high strain rates show significant changes compared to the other two loading rates. These results clearly demonstrate the importance of considering the loading rate effect in stress-
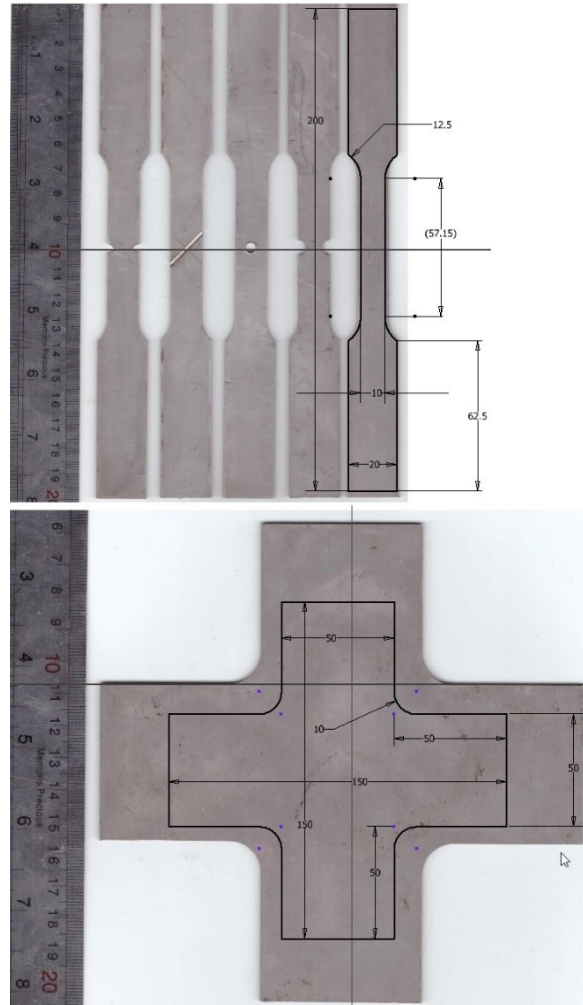

Fig. 1) Photos of the experimental samples manufactured with the wire cutting machine. a) Tensile samples with and without notch, b) equiaxial tensile sample
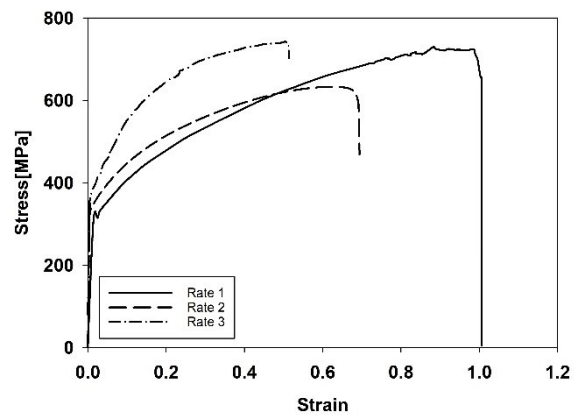

Fig. 2) Stress-strain responses at different loading strain rates

strain responses and as well as in the damage initiation of this type of alloy. As mentioned, in this research, samples with

different geometries have been used to create various stress states. To extract the ductile fracture constants, the results of biaxial tension tests and standard tension tests with semi-circular notches have been utilized. Separate experiments were conducted for each specimen in the 0°, 45°, and 90° directions. To extract the shear fracture constants, the results of biaxial tension tests, tension tests with a 1 mm deep groove in the 45° direction, and tension tests with a 1 mm deep groove parallel to the loading direction were used. To determine the triaxial stress state, finite element analysis is used to simulate the sample's behavior, capturing the stress distribution around the notch. Finally, the triaxiality is determined from the numerical results. In Figure 3, the experimental results for each direction of sample construction are presented under three different conditions of triaxiality. The selected samples cover a suitable range of triaxiality at the damage initiation point so that after this, in extracting the model coefficients and drawing the results, a reasonable range is available. Ultimately, the purpose of the model is to obtain the damage initiation range among these experimental data and beyond them in different orientations.

4- Data Fitting Using the Nonlinear Least Squares Method

In mechanical engineering, many physical phenomena are modeled using nonlinear relationships. To determine the parameters of such models based on experimental data, the nonlinear least squares (NLS) method is a powerful and reliable tool. This method aims to minimize the sum of squared deviations between observed data and the values predicted by a mathematical model. MATLAB provides an efficient implementation of this approach through the "nlinfit" function. A nonlinear relationship between the independent variable and the dependent variable expressed as equation 3 and 11, where is the mathematical model to be fitted to the data, $\beta = [\varepsilon_T^+, \varepsilon_T^-, c, f, \varepsilon_s^+$ and $\varepsilon_s^-]$ is the vector of model parameters to be estimated. The objective is to find the optimal parameters β that minimize the sum of squared residuals:

$$s(\beta) = \sum_{i=1}^{m} [y_i - f(x_i, \beta)]^2 \qquad (12)$$

where y_i are the experimental data points, $f(x_i, \beta)$ are the predicted values, and m is the number of data points. The NLS method typically uses iterative optimization algorithms such as the Gauss-Newton method to minimize S(β). Starting from an initial guess β_0, these algorithms refine the parameter estimates iteratively to reduce the residual sum of squares. In the Gauss-Newton method, the parameters are updated in each iteration as:

$$\beta^{(k+1)} = \beta^{(k)} - [J^T J]^{-1} J^T r \qquad (13)$$

Where J is the Jacobian matrix, containing partial derivatives of the model function with respect to the parameters and r is the residual vector, representing the difference between observed and predicted values. The Jacobian matrix plays a crucial role in the convergence of the algorithm, as it approximates the curvature of the residual function with respect to the parameters. The NLS method provides high accuracy in parameter estimation, particularly when the model closely represents the underlying physics of the

Table 2) Material parameters for the ductile fracture criterion in different loading rates based on equations (3) and (4)

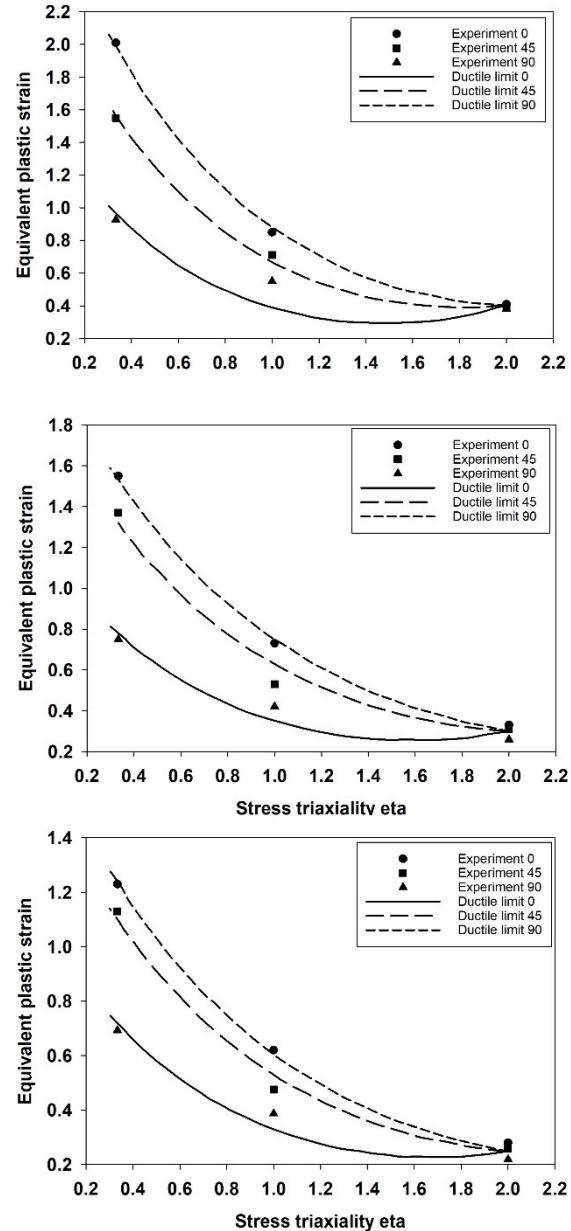| Parameter	Strain rates		
	Low	Mid	High
ε_T^+	0.4	0.3	0.25
ε_T^-	43	21	17
c	1.2928	1.1032	1.1014
k_0	1.4231	1.2129	1.1879
k_1	-0.1571	-0.1498	-0.1201
k_2	0.0268	0.0400	0.0336

Fig. 3) Ductile fracture limit curves, equivalent plastic strain versus stress triaxiality. Fitted curve and experimental data for low, mid and high strain rates (from top to bottom) in orientation of 0°, 45° and 90°

system. For this reason, some control point were fixed in the NLS code to consider the physical limit of the parameters.

5- Derivation of the fracture parameters

The NLS Matlab script has been used for fitting curves based on the equations (3) and the experimental results to extract the desired material parameters. The desired parameters are extracted separately for each loading rate, but the effect of loading direction on each set of coefficients has been considered. Therefore, three sets of coefficients have been obtained for the three loading rates, as presented in Table 2, for the ductile fracture criterion. Furthermore, in Figure 4, using the obtained coefficients, the onset of ductile failure limits is plotted, alongside experimental results for different loading rates. The results of plotting the damage initiation limit using the coefficients based on equations (3) and (4) for the ductile fracture case, considering the orientation effect. By changing the angle in equation (4), the damage initiation limit in other orientations where no experiment has been conducted can also be obtained using the obtained material parameters. In the shear fracture, the results yield a set of coefficients for each loading rate. However, in the shear fracture process, the failure mechanism is primarily governed by the local stress state, rather than void formation. The material undergoes shear deformation and eventually failure due to the critical shear stress, often resulting in the formation of shear bands, particularly in ductile materials. Anisotropic effects on shear failure are typically neglected in metals, but they must be considered in materials with directional properties, such as composites, where stress concentrations and failure modes may differ significantly along different directions[36], so in each case, only one graph of the damage initiation limit is considered. The obtained coefficients base on equation (11) are derived using an optimization process to achieve the best fit to the experimental data. During the fitting process, the physical nature of the coefficients must be taken into account. Table 3 presents the set of coefficients extracted for this criterion. The damage initiation limit is also illustrated in Figure 4 for each loading rate alongside the experimental data. In Figure 4, the experimental results for the shear fracture criterion are presented in three different conditions of triaxiality for biaxial test samples and tensile samples with inclined notches relative to the sample's longitudinal axis, as well as in the longitudinal direction. Using the obtained damage initiation limit, shown in Figures 3 and 4 for the ductile and shear cases respectively, it is possible to determine the critical plastic strain for damage initiation over a wide range of equivalent plastic strain, as well as for the ductile case in different directions. It is clear from the figures that the curve's fit to the experimental results shows good agreement.

4- Conclusion

Considering various effects such as loading rate and anisotropy in plastic behavior, as well as different failure criteria, is essential for predicting and ensuring the integrity of various components. Therefore, in this study, comprehensive experimental investigations have been conducted on the plastic behavior, shear fracture model, and ductile fracture model for stainless steel alloy 304. All specimens were extracted from steel sheets produced by rolling and using a wire cutting device. A variety of experiments were performed to investigate the effects of

Table 3) Obtained parameters for the shear fracture criterion at different loading rates

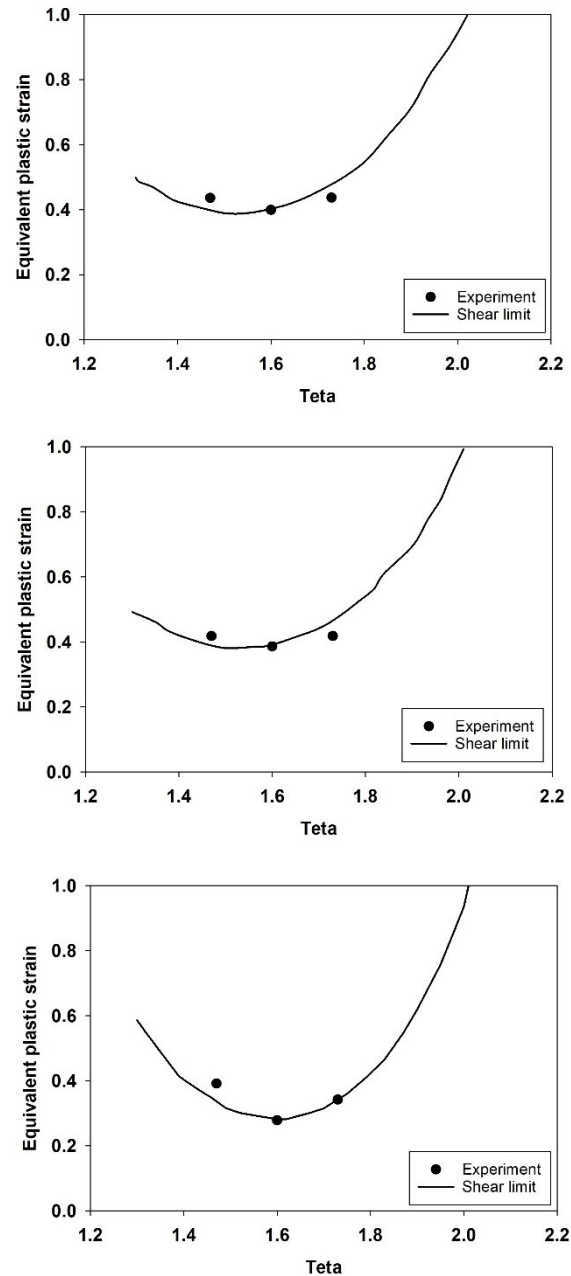| Strain rate	ε_s^+	ε_s^-	f	θ^+	θ^-
low	0.4	3.29	3.24	1.6	2.4
mid	0.39	3.41	3.32	1.6	2.4
high	0.28	5.98	4.67	1.6	2.4

Fig. 4) Shear fracture limit curves, equivalent plastic strain versus θ. Fitted curve and experimental data for low, mid and high strain rates (from top to bottom)

loading rate and triaxial stress state on the mentioned failure criteria. Finally, based on the obtained experimental results, ductile and shear fracture limit curves for the examined steel were obtained at low, medium, and high strain rates. The model used demonstrates the ability to reproduce experimental results over a wider range of equivalent plastic

strain and in different orientations. The experimental results highlight the importance of considering the effects of triaxiality and loading rates in the design, analysis, and ultimately the fabrication of any component with this alloy. The obtained results can be used to predict the onset of crack growth and damage in manufactured specimens or in various production processes of components made from stainless steel alloy 304 sheets.

Ethical Statement

The content of this manuscript is original, based on the authors' research, and has not been published or submitted elsewhere, either in Iranian or international journals.

Conflict of interest

The authors declared that they have no conflicts of interest to this work.

References

1- Lemaitre J. A continuous damage mechanics model for ductile fracture.

2- Gurson AL. Continuum theory of ductile rupture by void nucleation and growth: Part I—Yield criteria and flow rules for porous ductile media.

3- Sadeghi Nezhad MS, Haji Aboutalebi F, Mashayekhi M. Presentation of a new 2D fast and straightforward version for the Lemaitre's ductile damage model. Mechanics Based Design of Structures and Machines. 2024 Jan 2:1-29.

4- Salimpour E. Experimental determination and numerical implementation of ductile damage parameters of Al 2024-O. Modares Mechanical Engineering. 2018 Apr 10;18(2):45-52.

5- Khaleghi H, Amiri-Rad A, Mashayekhi M. A thermodynamically consistent continuum damage model for time-dependent failure of thermoplastic polymers. International Journal of Plasticity. 2022 Jul 1;154:103278.

6- Pijaudier-Cabot G, Bažant ZP. Nonlocal damage theory. Journal of engineering mechanics. 1987 Oct;113(10):1512-33.

7- Jirásek M. Non-local damage mechanics with application to concrete. Revue française de génie civil. 2004 Aug 1;8(5-6):683-707.

8- Bažant ZP, Jirásek M. Nonlocal integral formulations of plasticity and damage: survey of progress. Journal of engineering mechanics. 2002 Nov;128(11):1119-49.

9- de Borst R, Verhoosel CV. Damage, material instabilities, and failure. Encyclopedia of Computational Mechanics Second Edition. 2018 Feb 23:1-50.

10- Badnava H, Mashayekhi M, Kadkhodaei M. An anisotropic gradient damage model based on microplane theory. International Journal of Damage Mechanics. 2015;25(3):336-57.

11- Peerlings RH, de Borst R, Brekelmans WA, Geers MG. Gradient-enhanced damage modelling of concrete fracture. Mechanics of Cohesive-frictional Materials: An International Journal on Experiments, Modelling and Computation of Materials and Structures. 1998 Oct;3(4):323-42.

12- Peerlings RH, Geers MG, de Borst R, Brekelmans W. A critical comparison of nonlocal and gradient-enhanced softening continua. International Journal of solids and Structures. 2001 Nov 1;38(44-45):7723-46.

13- Badnava H, Mashayekhi M, Kadkhodaei M, Amiri-Rad A. A non-local implicit gradient-enhanced model for thermomechanical behavior of shape memory alloys. Journal of Intelligent Material Systems and Structures. 2018 May;29(9):1818-34.

14- Verhoosel CV, de Borst R. A phase-field model for cohesive fracture. International Journal for numerical methods in Engineering. 2013 Oct 5;96(1):43-62.

15- Badnava H, Msekh MA, Etemadi E, Rabczuk T. An h-adaptive thermo-mechanical phase field model for fracture. Finite Elements in Analysis and Design. 2018 Jan 1;138:31-47.

16- Badnava H, Etemadi E, Msekh MA. A phase field model for rate-dependent ductile fracture. Metals. 2017 May 17;7(5):180.

17- Marandi SM, Nourbakhsh SH, Dehkordi MB, Badnava H. Finite element implementation of coupled temperature-rate dependent fracture using the phase field model. Mechanics of Materials. 2020 Sep 1;148:103449.

18- Marandi SM, Badnava H, Dehkordi MB, Nourbakhsh SH. Phase-field modeling of coupled anisotropic plasticity–ductile fracture in rate-dependent solids. Journal of the Brazilian Society of Mechanical Sciences and Engineering. 2021 Apr;43:1-5.

19- Badnava H. Ductile fracture modelling based on the Drucker-Prager plasticity and phase field approach. Modares Mechanical Engineering. 2018 May 10;18(3):351-60.

20- Mousavion M, Mashayekhi M, Jamshidian M, Badnava H. Implementation of the phase-field method for brittle fracture and application to porous structures. Modares Mechanical Engineering. 2018 Nov 10;18(7):217-25.

21- Ganjiani M. A damage model incorporating dynamic plastic yield surface. Journal of Computational Applied Mechanics. 2016 Jun 1;47(1):11-24.

22- Aboutalebi FH. Numerical simulation of cutting and fine cutting processes by Lemaitre's ductile damage model in conjunction with large deformation theory. Modares Mechanical Engineering. 2013;13(6).

23- Ali Tavoli M, Gohari Rad S, Zajkani A, Darvizeh A. The Influence of Pre-Mechanical Friction Stir Processing on Stress State dependent Ductile Damage of 7075-T6 Aluminum Alloy. Modares Mechanical Engineering. 2017 Mar 10;17(1):365-74.

24- Zhou X, Feng B. A smeared-crack-based field-enriched finite element method for simulating cracking in quasi-brittle materials. Theoretical and Applied Fracture Mechanics. 2023 Apr 1;124:103817.

25- Kim MS, Kim HT, Choi YH, Kim JH, Kim SK, Lee JM. A new computational method for predicting ductile failure of 304L stainless steel. Metals. 2022 Aug 4;12(8):1309.

26- Othmen KB, Haddar N, Jegat A, Manach PY, Elleuch K. Ductile fracture of AISI 304L stainless steel sheet in stretching. International Journal of Mechanical Sciences. 2020 Apr 15;172:105404.

27- Abbassi F, Belhadj T, Mistou S, Zghal A. Parameter identification of a mechanical ductile damage using Artificial Neural Networks in sheet metal forming. Materials & Design. 2013 Mar 1;45:605-15.

28- Haghani M, Neya BN, Ahmadi MT, Amiri JV. Comparative study of smeared crack and extended finite element method for predicting the crack propagation in concrete gravity dams. Journal of Earthquake Engineering. 2022 Dec 10;26(16):8577-610.

29- Feist C, Hofstetter G. An embedded strong discontinuity model for cracking of plain concrete. Computer Methods in Applied Mechanics and Engineering. 2006 Nov 1;195(52):7115-38.

30- De Borst R. Numerical aspects of cohesive-zone models. Engineering fracture mechanics. 2003 Sep 1;70(14):1743-57.

31- Borst RD, Gutiérrez MA, Wells GN, Remmers JJ, Askes H. Cohesive-zone models, higher-order continuum theories and reliability methods for computational failure analysis. International Journal for Numerical Methods in Engineering. 2004 May 7;60(1):289-315.

32- Khoei AR. Extended Finite Element Formulation. Extended Finite Element Method 2014. p. 31-76.

33- Hooputra H, Gese H, Dell H, Werner H. A comprehensive failure model for crashworthiness simulation of aluminium

extrusions. International Journal of Crashworthiness. 2004 Sep 1;9(5):449-64.

34- El-Magd E, Gese H, Tham R, Hooputra H, Werner H. Fracture criteria for automobile crashworthiness simulation of wrought aluminium alloy components, Materialwissenschaft und Werkstofftechnik: Materials Science and Engineering Technology. 2001 Sep;32(9):712-24.

35- Johnson GR, Cook WH. Fracture characteristics of three metals subjected to various strains, strain rates, temperatures and pressures. Engineering fracture mechanics. 1985 Jan 1;21(1):31-48.

36- Besson J, Pineau A, Deschamps A. The role of microstructure in shear failure. International Journal of Fracture. 2001;109(1):3-23.